Journal of Electronic Materials, Vol. 18, No. 2, 1989

The Effect of Ion-Implantation Damage on Dopant Diffusion in Silicon During Shallow-Junction Formation

YUDONG KIM,[1] HISHAM Z. MASSOUD[1] and RICHARD B. FAIR[1,2]

[1]Department of Electrical Engineering
Duke University, Durham, N.C. 27706
[2]Microelectronics Center of North Carolina
Research Triangle Park, N.C. 27709

Low-thermal-budget annealing of ion-implanted BF_2^+, P, and As in Si was studied for shallow-junction formation. Implant doses were sufficient to amorphize the silicon surface region. Low-temperature furnace annealing and rapid-thermal annealing of ion-implanted boron, phosphorus and arsenic in silicon exhibit a transient enhanced diffusion regime resulting in junction depths considerably deeper than expected. The origin of this transient enhanced diffusion is the annealing of ion-implantation damage in the silicon substrate. We have found that point-defect generation during the annealing of either shallow end-of-range damage or small clusters of point defects dominates the transient enhanced diffusion process depending upon the annealing temperature and time. The net effect of damage annealing is to reduce the activation energy for dopant diffusion by an amount equal to the activation energy of the supersaturation of point defects in silicon. Models which can describe the transient enhancement characteristics in dopant diffusion during both furnace and rapid-thermal annealing of these implants are discussed.

Key words: Ion implantation, damage, diffusion, point defects, shallow junctions

INTRODUCTION

As lateral and vertical scaling of device dimensions continue in order to increase packing density and speed, and reduce power consumption, it is critical to form shallow junctions for submicron MOS VLSI device structures.[1,2] Ion implantation is the most widely used technology for introducing dopants into the substrate during the fabrication of shallow junctions. Shallow n^+p junctions are formed by As implantation, and p^+n junctions by BF_2^+ molecular implantation.[3–5] The relatively high diffusivity and channeling of boron during implantation make it challenging to form shallow p^+n junctions.[6,7] The main restriction on implant annealing in the fabrication of shallow junctions is to minimize the product of dopant diffusivity and diffusion time. Rapid-thermal annealing (RTA) and low-temperature furnace annealing are two possible methods of achieving shallow junctions in conjunction with ion implantation.[8–10] However, the transient enhanced diffusion of implanted dopants in silicon was observed during RTA as well as furnace anneal, which produces significantly deeper junction depths than expected.[11–13] Especially, ion-implanted boron in silicon exhibits transient enhanced diffusion which exceeds the equilibrium diffusivity as much as 1000×.[14] The initial transient enhanced diffusion of *implanted dopants in silicon arises from point-defect* generation process during the annealing of implantation damage.[15–17]

This paper describes the experimental results obtained by extensive SIMS profiling of dopants with annealing time, temperature, furnace ambient, implanted dose and dopant species as variables. Cross-section TEM studies were also done to understand the role of ion-implantation damage annealing on dopant diffusion. In our experiments, the implant dose and mass were high enough to generate surface amorphization. In general, we have found that the magnitude of diffusion enhancement and the time duration of the enhancement are related to the type of damage produced. Depending upon the annealing temperature and time, the annealing of a certain type of implantation damage becomes dominant and results in unique dopant profiles. A general relation between implantation damage annealing and dopant diffusion will be established. The experimental results and the models describing the transient enhancement characteristics of the dopant diffusion will be also discussed.

DOPANT DIFFUSION AND DAMAGE ANNEALING

Damage assisted or retarded diffusion of ion-implanted dopants in silicon depends on (a) the type of damage introduced by implantation and point-defect generation characteristics during annealing,[18] (b) the location and distribution of the damage,[15] and (c) the dominant diffusion mechanism by which the dopant diffuses. For instance, boron and phosphorus are believed to diffuse primarily via a self-interstitialcy mechanism which involves silicon self-interstitials, antimony has a significant vacancy mechanism involving vacancies as manifested by the oxidation-enhanced (OED) and oxidation-retarded (ORD) diffusion phenomena, and

(Received August 17, 1988; revised December 6, 1988)

arsenic diffuses via a combination of vacancy and self-interstitialcy mechanisms.[19–21]

Depending upon the dose and species, ion implantation can produce different types of damage as shown in Fig. 1, which summarizes implant damage depending on the implant dose and mass.[18] When the implant is of such a dose and mass that surface amorphization occurs, several kinds of defects can be produced as shown in Fig. 1(a). Vacancy-type defects can be produced near the surface as revealed by multiple crystal X-ray diffraction,[15,22] category II or end-of-range damage can be produced just beyond the original amorphous/crystalline interface,[23] and interstital-type defects may also be distributed throughout the implanted layer. Figure 1(b) shows the implant damage in high-dose boron implants when no amorphization occurs. The category V or projected-range damage can be produced at the peak of the implant if the peak concentration exceeds the dopant solid solubility at the annealing temperature,[23] and interstitial-type defects may also be distributed beyond the projected range. Defect distribution in ion-implanted silicon is also obtained by Mazzone[25] using Monte Carlo simulation, which is consistent with the results from multiple crystal X-ray diffraction studies.[26]

Each of these types of defects exhibit its own annealing characteristics as shown in Fig. 2, where the annealing temperature dependence of the time required to anneal deep dislocations at the end of range, which is deeper than 1000Å from the surface, or small clusters of point defects is plotted.[27] Both damage annealing characteristic curves show the 5 eV activation energy associated with the diffusion of self-interstitials or vacancies during the anneal process.[28,29] A much shorter time is required for the removal of point-defect clusters than that of deep end-of-range dislocations. This graph suggests that, for example, during rapid-thermal annealing around 900° C, the dominant point-defect generator may be isolated point-defect clusters, whereas at

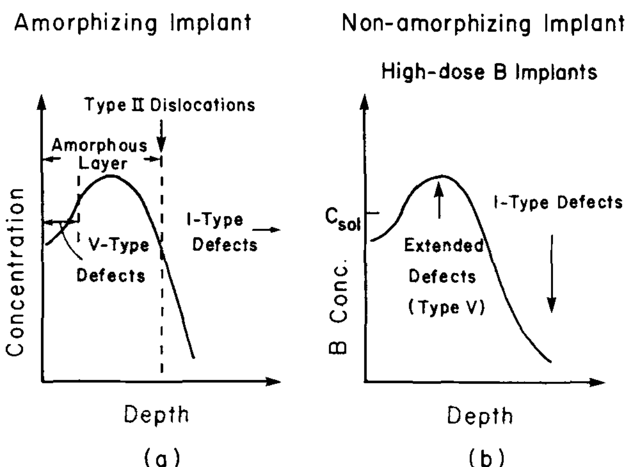

Fig. 1 — Defect production processes in ion-implanted silicon, (a) when implant dose and mass are sufficient to cause surface amorphization, and (b) when implant dose is high but no amorphization occurs, such as in high-dose B implants.

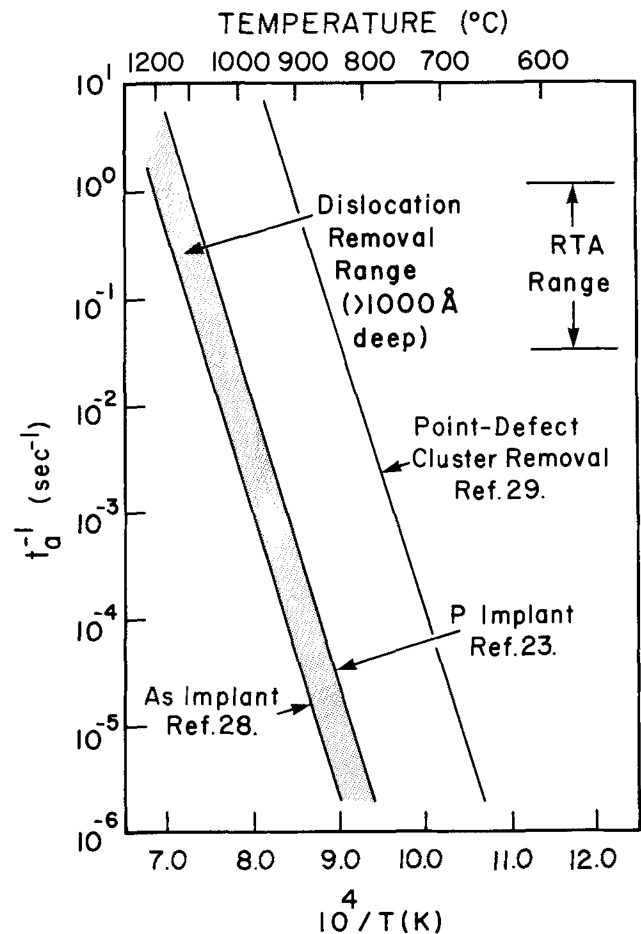

Fig. 2 — Temperature dependence of the damage-annealing time constant t_a.

temperatures above 1000° C, deep end-of-range dislocations may become more important.

EXPERIMENTAL PROCEDURES

Czochralski-grown, (100)-oriented, 50 Ω-cm *p*-type silicon wafers were thermally oxidized to grow 140Å of SiO_2. Ion implantations were done through the SiO_2 layer at an energy of 40 keV for three common dopants: BF_2^+, phosphorus and arsenic with the ion beam normal to the surface at room temperature. Doses of BF_2^+ and arsenic were 2×10^{14}, 7×10^{14}, and 2×10^{15} cm^{-2}. Phosphorus implant doses were 1×10^{14}, 3×10^{14}, and 1×10^{15} cm^{-2}. Anneals were done in a furnace at temperatures ranging from 650° C to 850° C for times varying from 30 to 240 min. Rapid-thermal annealings were performed at 900° C for 15 to 60 sec. The annealing ambient was generally nitrogen but some annealing treatments were done in dry O_2. Surface oxides were etched in a buffered HF solution and SIMS dopant depth profile measurements were made in a CAMECA-ims3f system. Every profile was reproduced to ensure that the ion probe was in proper and stable operating condition. Cross-section TEM was used to track the morphology changes of the implant damage upon annealing. The dopant diffusion was also simulated using PREDICT™.[18]

EXPERIMENTAL RESULTS

High-dose BF_2^+ Implantation:

1. Low-Temperature Furnace Annealing:

For a high-dose BF_2^+ implant resulting in surface amorphization, Fig. 3 shows a typical example of the dopant profiles, obtained by SIMS and simulated by PREDICT,[18] after conventional furnace annealing at 750° C and 850° C for 1 hr. There is little diffusion in the high-concentration region near the surface. The location of end-of-range damage is indicated by a plateau at about 550Å from the surface,[30] and the enhanced diffusion tails begin at a concentration determined by the annealing temperature. In the tail regions, the diffusion coefficients are very large and the shape of the tail is modified by the initial transient in the enhanced diffusion associated with the annealing of the shallow end-of-range damage. For example, at 750° C, the time for the enhanced diffusion is about 30 min, whereas at 850° C it may be less than 1 min. Therefore, even though both 850° C and 750° C anneals for 1 hr produced the same junction depth of 0.25 μm at a concentration level of 1×10^{16} cm^{-3}, it is not athermal diffusion and the time constant for the enhanced diffusion makes it appear that boron moved to the same depth. Figure 4 shows the SIMS boron diffusion profiles obtained after 30, 60, and 240 min anneals at 750° C. It is seen that the initial transient time for enhanced B diffusion is on the order of 30 min, as the 60 and 240 min profiles coincided with the 30 min profile.

An experiment was performed to verify that the origins of point defects for the enhanced tail diffusion are in fact in the near-surface region where the implant damage is located. About 800Å of the as-implanted silicon surface was etched using DASH etch,[31] which is a solution of $HF:HNO_3:CH_3COOH$ with the volume ratios of 1:3:10. The etched step

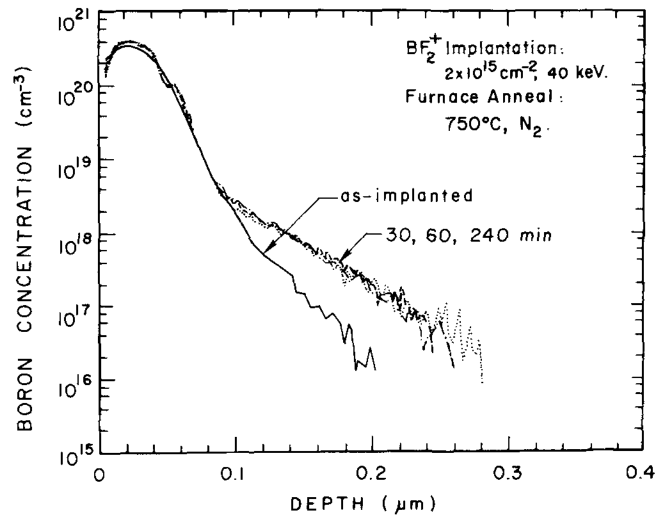

Fig. 4 — SIMS boron profiles for 2×10^{15} cm^{-2} BF_2^+ implanted in (100) silicon at 40 keV, and annealed in nitrogen at 750° C for 30, 60, and 240 min.

depth was measured using a surface profilometer, which gave a value close to that obtained by SIMS when comparing the depth of the tail region. Various anneals were used on the etched samples, such as a furnace anneal at 750° C for 30 min, RTA at 900° C for 30 sec, and a combined anneal of RTA at 900° C for 30 sec and furnace annealing at 850° C for 1 hr. The results are shown in Fig. 5, and indicate that no sample annealed under the above mentioned conditions showed any enhanced diffusion. This result confirms that the sources of point defects responsible for the enhanced tail diffusion are in the near-surface region. A similar result was obtained by Fan *et al.*[32] for 1×10^{15} cm^{-2}, 50 keV, B^+ implants.

In order to understand the role of ion-implantation damage in the surface region on dopant diffusion, cross-section TEM was also used, and revealed

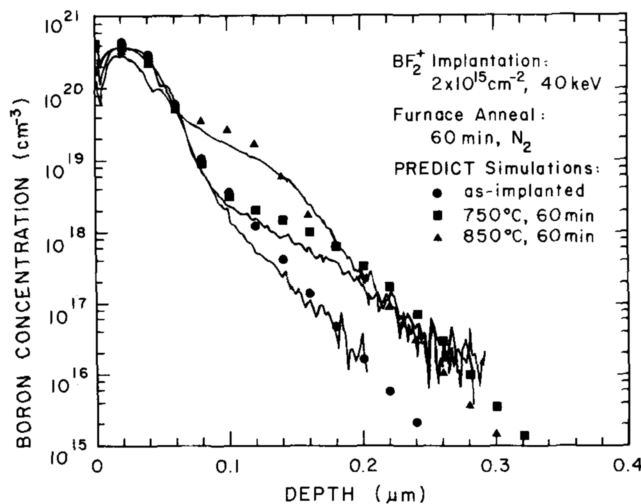

Fig. 3 — SIMS boron profiles for 2×10^{15} cm^{-2} BF_2^+ implanted in (100) silicon at 40 keV, and annealed in nitrogen for 60 min at 750° C and 850° C. Simulation results using PREDICT 1.3 are also shown.

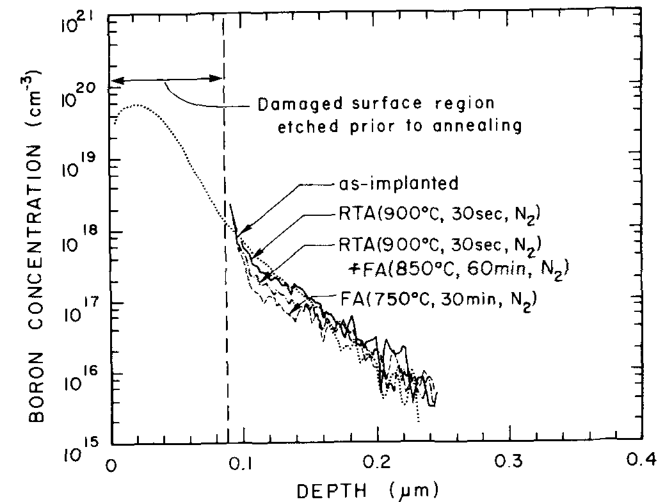

Fig. 5 — SIMS boron profiles for 2×10^{14} cm^{-2} BF_2^+ implanted in (100) silicon at 40 keV, and annealed after etching 800Å of the as-implanted Si surface to remove the near-surface region damaged by ion implantation.

that a 2×10^{14} cm^{-2} BF_2^+ implant at 40 keV through 140Å of SiO_2 produces about 300Å of amorphous silicon layer. After a 30 min anneal at 650° C, end-of-range dislocations are formed at about 400Å below the Si-SiO_2 interface. When annealed for 30 min at 750° C, the small dislocation loops at the end-of-range coalesce and grow into larger loops. This corresponds to the time at which the enhanced diffusion transient stops. After a 30 min anneal at 850° C, the large loops disappear and only small loops remain. This is well past the time when the enhanced diffusion occurs.[30]

2. Rapid-Thermal Annealing:

As the annealing temperature is increased during RTA, a substantially shorter time constant associated with the enhanced diffusion was observed. This may be an indication of some other type of point-defect source being involved in the high-temperature regime. Figure 6 shows the time dependence of boron diffusion during RTA at 900° C for 15, 30 and 60 sec. It can be seen that the enhanced diffusion of boron has diminished and is almost over after 30 sec. However, if a furnace anneal at 850° C for 1 hr is performed following RTA, substantial additional diffusion is observed, as shown in Fig. 7. Therefore, although the enhanced diffusion time constant during RTA seems to have ended, there is still enough residual damage to cause an additional enhanced diffusion during furnace annealing at lower temperatures. A plateau at about 500Å below the surface in the dopant depth profile indicates that the end-of-range damage is still present after RTA.

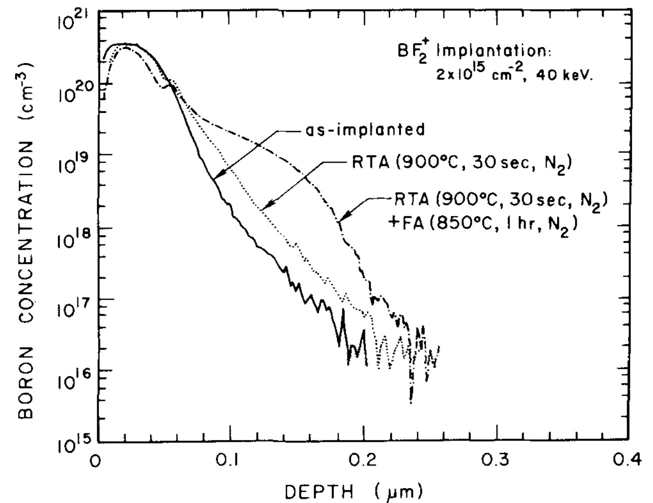

Fig. 7 — SIMS boron profiles for 2×10^{15} cm^{-2} BF_2^+ implanted in (100) silicon at 40 keV, and rapid-thermal annealed in nitrogen at 900° C for 30 sec, and RTA at 900° C for 30 sec plus furnace annealed at 850° C for 1 hr.

High-Dose As and P Implantation:

1. Low-Temperature Furnace Annealing:

An initial transient is observed for arsenic annealed at 750° C for 30, 60 and 240 min, as shown in Fig. 8. It should be noted that after a 30 min anneal at 750° C, there is little change in the profile. Cross-section TEM micrographs in Fig. 9 show that only small dislocation loops remained after annealing at 750° C for 30 min. Therefore, the time constant for transient enhanced diffusion of arsenic under this annealing condition is less than 30 min. The initial transient enhanced diffusion for phosphorus during low-temperature furnace anneal cycles was also observed as shown in Fig. 10. The time constant for transient enhancement is also less than 30 min at 750° C. It is noted that the junction depths at a concentration level of 1×10^{16} cm^{-3} are deeper than 0.5 μm.

2. Rapid-Thermal Annealing:

The initial transient for arsenic is observed during RTA. Figure 11 shows that the time constant

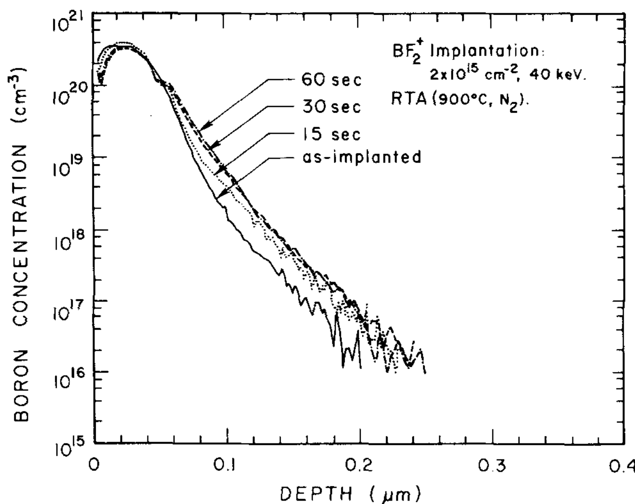

Fig. 6 — SIMS boron profiles for 2×10^{15} cm^{-2} BF_2^+ implanted in (100) silicon at 40 keV, and rapid-thermal annealed in nitrogen at 900° C for 15, 30 and 60 sec.

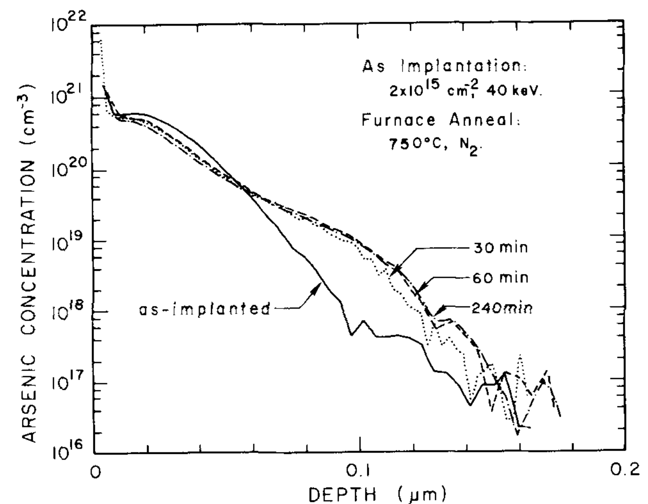

Fig. 8 — SIMS arsenic profiles for 2×10^{15} cm^{-2} As implanted in (100) silicon at 40 keV, and annealed in nitrogen at 750° C for 30, 60 and 240 min.

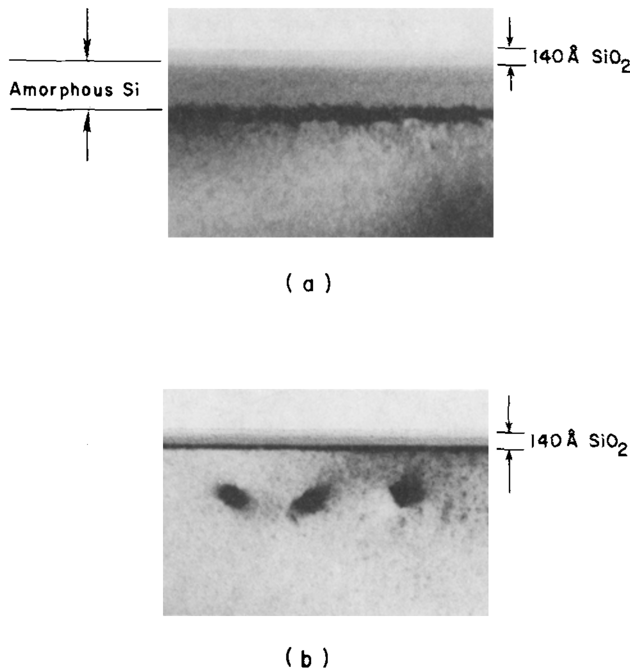

Fig. 9 — Cross-sectional TEM micrographs of the damaged surface region as a result of 2×10^{15} cm^{-2} As implant into (100) silicon at 40 keV, (a) as-implanted, and (b) annealed in nitrogen at 750° C for 30 min.

for the transient enhancement is much less than 15 sec. There is very little change in profile after 15 sec at 900° C. However, low-temperature furnace annealing of rapid-thermal annealed samples show an additional diffusion which is similar to that observed for the BF_2^+ implants.

An initial transient during RTA is also observed for phosphorus, and the time constant for the transient enhancement is also less than 15 sec as shown in Fig. 12. The combined RTA plus furnace anneal also shows an additional diffusion for phosphorus. The junction depth obtained by RTA at a concentration level of 1×10^{16} cm^{-3} is 0.35 μm.

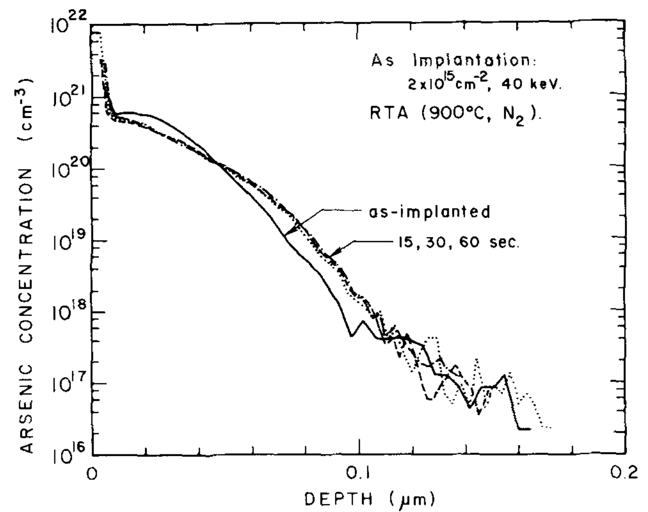

Fig. 11 — SIMS arsenic profiles for 2×10^{15} cm^{-2} As implanted in (100) silicon at 40 keV, and annealed in nitrogen at 900° C for 15, 30 and 60 sec.

DISCUSSION AND MODELING

Based on SIMS profiling and cross-section TEM, a model which can describe the transient enhancement in the diffusion of high-dose implanted BF_2^+ is proposed as follows. The end-of-range dislocations are formed initially during annealing by the point defects diffusing from the amorphous layer. Evolution of the end-of-range damage from supersaturation of point defects to extrinsic dislocation loops upon annealing can be envisaged using the model proposed by Tan.[33] A row of interstitial atoms each with two broken bonds forms intermediate defect configurations having non-six-membered atomic rings with matrix crystal atoms to minimize the numbers of dangling bonds. Climb and glide motion of these intermediate defect configurations produce dislocation loops. According to Prussin *et al.*,[34] the number of point defects that escape the amorphous

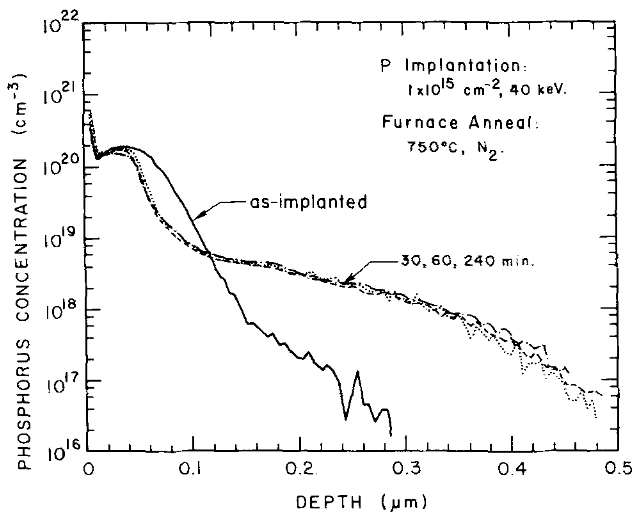

Fig. 10 — SIMS phosphorus profiles for 1×10^{15} cm^{-2} P implanted in (100) silicon at 40 keV, and annealed in nitrogen at 750° C for 30, 60 and 240 min.

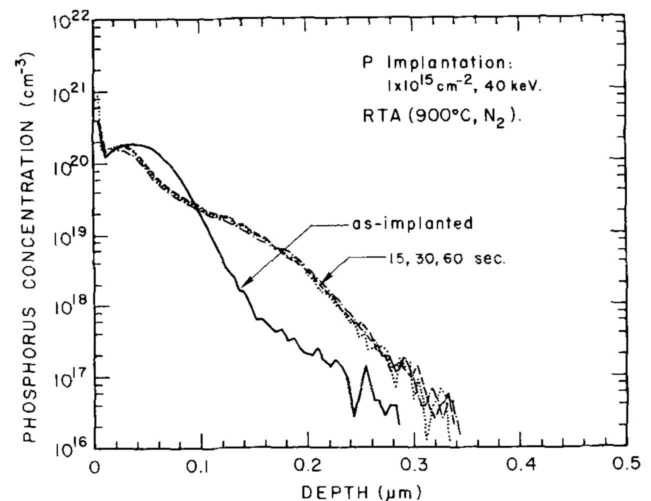

Fig. 12 — SIMS phosphorus profiles for 1×10^{15} cm^{-2} P implanted in (100) silicon at 40 keV, and annealed in nitrogen at 900° C for 15, 30 and 60 sec.

layer is a function of the mass of the implanting ion. Therefore, the heavier the mass, the more dislocation loops are expected to form. During annealing, these small loops at the end of range coalesce to form larger loops through dislocation-dislocation reactions and nonconservative climb processes.[35] In general, the nonconservative climb motion of dislocations requires generation of point defects when the dislocation moves out of the glide plane determined by the dislocation line and the Burgers vector.[36] Therefore, while these loops are growing, point defects are being produced. But when the loops reach a certain critical size, the attractive interaction force between dislocation loops and a free surface or interface becomes large enough to pull these loops out of the surface via a glide mechanism in spite of the lattice frictional force in the crystal. It is believed that the point-defect generation transient ends when these large loops are quickly pulled out of the surface via glide motion in which the dislocation moves in the glide plane. The interaction force can be either attractive or repulsive dependent upon whether the second phase is softer or harder, respectively.[37] The glide process of the end-of-range dislocations to the surface had been observed by Wu *et al.*[38] It is important to note that dislocation loops have to be located within twice their diameter from the surface in order for the interaction force to be sufficient to pull them out of the crystal. Therefore, it is expected that this mechanism only applies to either dislocations within 1000Å of the surface or those with large diameters. Similar results were obtained earlier by Ajmera *et al.*[39] who observed that the dislocation loops just under the mask edge near the surface were annihilated, whereas the deeper dislocation loops remained after annealing. The rapid diappearance of shallow dislocations on the order of 400Å from the surface was observed to have an activation energy on the order of 1.5 to 2.5 eV in this study. A rapid annihilation of surface stacking faults has also been observed to have a 2.3 eV activation energy.[40]

There is a correlation between the enhanced-diffusion transient and the fast disappearance of shallow dislocation loops at the end of range. Figure 13 shows the temperature dependence of the transient-enhanced-diffusion time constant T_D for BF_2^+ implants and that required to dissolve the shallow end-of-range dislocations t_a. From 750° C to 850° C, we observed that the transient-enhanced-diffusion time constant is within the uncertainty of the dissolution time constant for shallow end-of-range dislocations. Therefore, it would appear that the time constant for the enhanced diffusion coincides with the dissolution time constant for shallow end-of-range dislocations.

A short transient was observed during RTA. It was also found that RTA followed by furnace anneal results in additional diffusion. The short transient seems to be due to point-defect generation during the annealing of isolated point-defect clusters. During RTA, we found that the diffusion activation energy for boron is reduced by roughly 2 eV which is consistent with the temperature dependence of the supersaturation of self-interstitials generated by thermal oxidation reported by Antoniadis.[41]

The results of combined RTA plus furnace annealing indicate that there are two different sources of point defects which cause the transient enhance-

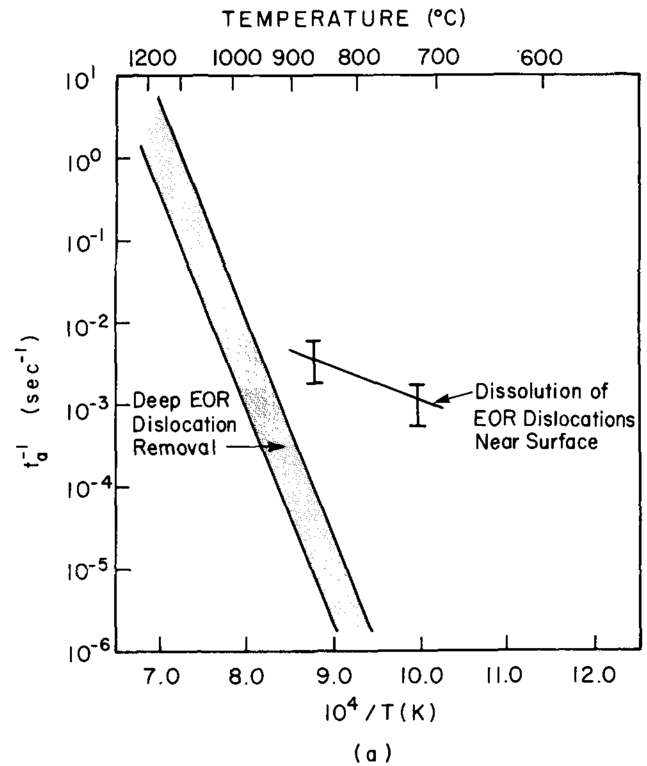

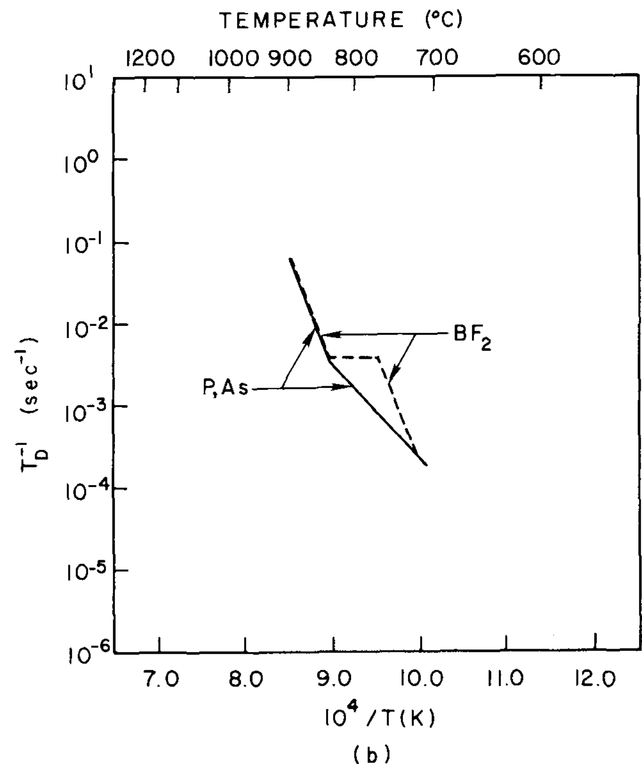

Fig. 13 — Temperature dependence of (a) the time constant of implant damage anneaing (t_a) and (b) the transient enchanced diffusion (T_D) of BF_2^+, P and As in Si.

ment in boron diffusion. During RTA at 900° C, the dominant point-defect source is the annealing of small point-defect clusters, which results in an enhanced-diffusion transient shorter than 30 sec. Furnace annealing at 850° C for 1 hr following RTA allows another point-defect source, *i.e.* shallow end-of-range dislocations, to participate in the diffusion process which gives an additional diffusion of boron after the end of the RTA transient.

In the phosphorus and arsenic diffusion studies, the temperature dependence of the time constant for enhanced diffusion during furnace anneals indicates that both phosphorus and arsenic show almost the same time constant, which also coincides with the time constant for BF_2^+ as shown in Fig. 13. However, arsenic and phosphorus differ from BF_2^+ below 850° C and converge at lower temperatures. During low-temperature furnace annealing, the time constants are similar to the damage annealing time for Si-amorphization into predeposited boron and phosphorus layers as pointed out by Angelucci *et al.*[42] indicating that end-of-range damage annealing is the dominant point-defect source. It is expected that the transient enhancement in arsenic and phosphorus diffusion during furnace anneals would have a similar mechanism to that observed in the BF_2^+ implants. However, comparing TEM micrographs of BF_2^+- and As-implanted samples which have undergone the same furnace annealing at 750° C for 30 min, it was found that As implants have a much faster annealing time of shallow end-of-range dislocations than BF_2^+ implants.

During rapid-thermal annealing, both phosphorus and arsenic show an initial transient with a time constant smaller than 15 sec at 900° C. This is associated with the annealing of isolated point-defect clusters. The net effect of damage annealing is to reduce the diffusion activation energy by 2.1 to 2.5 eV. An activation energy reduction of about 2.5 eV was also observed by Tsai *et al.*[43] who reported a reduction in the activation energy of the diffusion of an As buried layer when high-concentration phosphorus is present. Phosphorus diffusion at concentrations above solid solubility is known to generate silicon self-interstitials.[44]

The combined RTA plus furnace annealing of phosphorus and arsenic implants also results in additional diffusion when compared to RTA only. However, the degree of additional movement of phosphorus and arsenic is not as dramatic as that of boron. A mechanism, similar to that present in the BF_2^+ implant annealing, is expected to be operative for phosphorus and arsenic implants considering that the same implant damage structure, *i.e.* surface amorphization, is present in all three implants. However, it is conjectured that there might be a difference in the resultant diffusion profile due to the difference in annealing characteristics of implant damage when different dopants are present. Prussin and Jones[45,46] have reported that the defect annealing kinetics can be affected by the implant species via the stress induced by the difference in tetrahedral covalent radii, the electrical field and charge concentration, and impurity diffusion mechanisms.

CONCLUSIONS

Low-thermal-budget annealing of ion-implanted BF_2^+, phosphorus, and arsenic were investigated for the fabrication of shallow junctions. Ion-implantation damage annealing dominates the initial diffusion for low-thermal-budget processes. Diffusion during low-temperature furnace annealing below 850° C is dominated by point-defect generation from shallow end-of-range dislocations. The transient characteristics of point-defect generation can be modeled by the interaction between small dislocation loops at the end of range and its quick glide motion to the surface. During the short-time high-temperature diffusion present in RTA, the annealing of point-defect clusters seems to dominate. The combination of RTA and furnace annealing of BF_2^+ implants clearly shows that there are at least two different point-defect sources with different annealing characteristics depending on annealing temperature and time. For all dopants studied, the effect of damage annealing is to reduce the activation energy of dopant diffusion in silicon by 2.5 eV, the energy required to form silicon self-interstitials. For accurate low-thermal-budget process modeling, the characterization of the spatial distribution and type of implant damage, the point-defect generation process, the implant parameters and other sources of point defects such as injection of silicon self-interstitials during oxidation must be included.

ACKNOWLEDGMENTS

This work was supported by a grant from Intel Corporation. The authors would especially like to thank Dr. Rajiv Mathur for his continued interest and support. Special thanks are due to Dr. D. Griffis of North Carolina State University for his help and assistance with SIMS profiling, and to Dr. S. Chevacharoeukul of Microelectronic Center of North Carolina for transmission microscopy.

REFERENCES

1. M. C. Ozturk and J. J. Wortman, Appl. Phys. Lett. *52,* 281 (1988).
2. Y. El-Mansy, IEEE Trans. Electron Devices ED-*29,* 567 (1982).
3. H. Müller, H. Ryssel and I. Ruge, in *Ion Implantation in Semiconductor,* edited by I. Ruge and J. Graul, p. 85, Spring-Verlag, Berlin, 1971.
4. N. C. Tung, J. Electrochem. Soc. *132,* 914 (1985).
5. D. E. Davies, IEEE Electron. Dev. Lett., *6,* 397 (1985).
6. T. O. Sedgwick, Mater. Res. Soc. Symp. Proc. *71,* 403 (1986).
7. B. L. Crowder, J. F. Ziegler and G. W. Cole, in *Ion Implantation in Semiconductors and Other Materials,* edited by B. L. Crowder, p. 257, Plenum, New York, 1973.
8. R. Kwor, D. L. Kwong and Y. K. Yeo, Appl. Phys. Lett. *45,* 77 (1984).

9. J. B. Lasky, J. Appl. Phys. *54,* 6009 (1983).
10. T. O. Sedgwick, R. Kalish, S. R. Mader and S. C. Shatas, Mat. Res. Soc. Symp. Proc. *23,* 293 (1984).
11. W. K. Hofker, H. W. Werner, D. P. Oosthoek and H. A. M. de Grefte, Appl. Phys. *2,* 265 (1973).
12. R. T. Hodgson, V. R. Deline, S. M. Mader and J. C. Gelpey, Appl. Phys. Lett. *44,* 589 (1984).
13. T. O. Sedgwick, J. Electrochem. Soc. *130,* 484 (1983).
14. M. Miyake and S. Aoyama, J. Appl. Phys. *63,* 1754 (1988).
15. M. Servidori, R. Angelucci, F. Cembali, P. Negrini, S. Solmi, P. Zaumseil, and U. Winter, J. Appl. Phys. *61,* 1834 (1987).
16. S. J. Pennycook, J. Narayan and O. W. Holland, J. Electrochem. Soc. *132,* 1962 (1985).
17. A. E. Michel, W. Rausch, P. A. Ronsheim and R. H. Kastl, Appl. Phys. Lett. *50,* 416 (1987).
18. R. B. Fair, IEEE Trans. Electron Devices ED-*35,* 285 (1988).
19. D. A. Antoniadis, A. M. Lin and R. W. Dutton, Appl. Phys. Lett. *33,* 1030 (1978).
20. S. Mizuo and H. Higuchi, Jpn. J. Appl. Phys. *20,* 739 (1981).
21. R. M. Harris and D. A. Antoniadis, Appl. Phys. Lett. *43,* 937 (1983).
22. S. Solmi, R. Angelucci, F. Cembali, M. Servidori, and M. Anderle, Appl. Phys. Lett. *51,* 331 (1987).
23. K. S. Jones, S. Prussin, and E. R. Weber, J. Appl. Phys. *62,* 4114 (1987).
24. T. O. Sedgwick, A. E. Michel, V. R. Deline, S. A. Cohen and J. B. Lasky, J. Appl. Phys. *63,* 1452 (1988).
25. A. M. Mazzone, Phys. Status Solidi (A) *95,* 149 (1986).
26. M. Servidori, P. Zaumseil, U. Winter, F. Cembali and A. M . Mazzone, Nucl. Inst. Methods Phy. Res. B .22, 497 (1987).
27. R. B. Fair, Abstract No. 194, Extended Abstracts of the Spring Meeting of the Electrochemical Society, Vol. 88-1, p. 303, The Electrochemical Society, Pennington, New Jersey, 1988.
28. T. E. Seidel, D. J. Lischner, C. S. Pai, R. V. Knoell, D. M. Maher and D. C. Jacobson, Nucl. Inst. Methods Phys. Res. B *7/8,* 251 (1985).
29. T. E. Seidel and A. U. MacRae, Rad. Effects *7,* 1 (1973).
30. Y. Kim, H. Z. Massoud and R. B. Fair, Appl. Phys. Lett. *53, 2197 (1988).*
31. J. F. Gibbons, E. O. Hechtl and T. Tsurushima, Appl. Phys. Lett. *15,* 117 (1969).
32. D. Fan, J. Huang, R. J. Jaccodine, P. Kahora and F. Stevie, Appl. Phys. Lett. *50,* 1745 (1987).
33. T. Y. Tan, Phil. Mag. A *44,* 101 (1981).
34. S. Prussin and K. S. Jones, Abstract No. 176, Extended Abstracts of the Spring Meeting of the Electrochemical Society, Vol. 88-1, p. 271, The Electrochemical Society, Pennington, New Jersey, 1988.
35. R. B. Fair, J. J. Wortman and J. Liu, J. Electrochem. Soc. *131,* 2387 (1984).
36. J. D. Verhoeven, *Fundamentals of Physical Metallurgy,* John Wiley & Sons, Inc., New York, 1975.
37. J. Narayan and K. Jagannadham, J. Appl. Phys. *62,* 1694 (1987).
38. N. R. Wu, P. Ling, D. K. Sadana, J. Washburn and M. I. Current, *Defects in Silicon,* Electrochemical Society Proceedings Vol. 83, edited by W. M. Bullis and L. C. Kimmerling, p. 363, The Electrochemical Society, Pennington, New Jersey, 1983.
39. A. C. Ajmera and G. A. Rozgonyi, Appl. Phys. Lett. *49,* 1269 (1986).
40. K. Nishi and D. A. Antoniadis, Appl. Phys. Lett. *46,* 516 (1985).
41. D. A. Antoniadis, J. Electrochem. Soc. *129,* 1093 (1982).
42. R. Angelucci, F. Cembali, P. Negrini, M. Servidori and S. Solmi, J. Electrochem. Soc. *134,* 3130 (1987).
43. J. C. C. Tsai, D. G. Schimmel, R. B. Fair and W. Maszara, J. Electrochem. Soc. *134,* 1508 (1987).
44. H. Strunk, U. Gösele and B. O. Kolbesen, Appl. Phys. Lett. *34,* 530 (1979).
45. S. Prussin and K. S. Jones, Nucl. Inst. Methods Phy. Res. B *21,* 496 (1987).
46. K. S. Jones, S. Prussin and E. R. Weber, Nucl. Inst. Methods Phy. Res. B *21,* 499 (1987).